Journal of Micromechanics and Microengineering

Evaluation of the impact of abnormal grains on the performance of $Sc_{0.15}Al_{0.85}N$-based BAW resonators and filters

OPEN ACCESS
IOP Publishing
Journal of Micromechanics and Microengineering
J. Micromech. Microeng. **32** (2022) 034002 (10pp)
https://doi.org/10.1088/1361-6439/ac4826

Evaluation of the impact of abnormal grains on the performance of $Sc_{0.15}Al_{0.85}N$-based BAW resonators and filters

Chen Liu, Minghua Li, Bangtao Chen, Ying Zhang, Yao Zhu and Nan Wang*

Institute of Microelectronics, A*STAR (Agency for Science, Technology and Research), Singapore

E-mail: wangn@ime.a-star.edu.sg

Received 4 October 2021, revised 1 December 2021
Accepted for publication 5 January 2022
Published 28 January 2022

Abstract

$Sc_xAl_{1-x}N$ is a promising piezoelectric material for radio frequency communication applications with excellent electro-acoustic properties. However, the growth of abnormally oriented grains is widely observed in the Sc doped AlN films deposited by sputtering. In this work, for the first time, the impact of the abnormal grains in the $Sc_{0.15}Al_{0.85}N$ films on the performance of bulk acoustic wave resonators and filters is systematically evaluated by both simulations and measurements. The correlation between the device performance and the abnormal grain parameters, including the density, dimension, crystal orientation, growth height and the total volume of the abnormal grains, is evaluated and quantified. Simulation results show that the total volume of all abnormal grains in the whole device is the most critical factor among the parameters. Abnormal grains with randomly distributed parameters and around 6% total volume of the film can degrade the effective coupling coefficient of the resonator from 13.6% to 11%, leading to a 10.6% decrement of the filter bandwidth. Wafer-level device characterizations and measurements are performed, and the results are consistent with the simulations. This study provides a practical method for predicting the performance of the resonators and filters with abnormal grains, and a guideline for film quality evaluation.

Keywords: piezoelectric, ScAlN, abnormally oriented grain, resonator, filter

(Some figures may appear in colour only in the online journal)

1. Introduction

Wide frequency bands introduced by 5G new radio such as n77 to n79 require radio-frequency (RF) frontend filters with significantly higher bandwidth. To achieve the increased bandwidth without comprising the out-of-band rejection and in-band insertion and return loss, the acoustic resonators inside the filters needs to provide a much higher effective coupling coefficient (k^2_{eff}), which can no longer be achieved by conventional Aluminum Nitride (AlN) based bulk acoustic wave (BAW) resonators [1–3]. So far, a promising approach widely accepted by industry is to dope Scandium (Sc) into AlN ($Sc_xAl_{1-x}N$) to increase the material's intrinsic longitudinal piezoelectric response [4–10]. However, structure distorted defects, known as abnormal grains, generally exist in the $Sc_xAl_{1-x}N$ films with more than 15% Sc. Research efforts have been devoted to investigate the inducements of

* Author to whom any correspondence should be addressed.

the abnormal grains and the approaches to suppress the abnormal grains. Increasing Sc concentration has been confirmed to facilitate the growth of the abnormal grains [11–13]. Film stress is also identified to be another critical parameter for the amount of the abnormal grains and a compressive stress is believed to have a positive impact on the elimination of the grains [14, 15]. Possible approaches to suppress the abnormal grains in the $Sc_xAl_{1-x}N$ films include tuning of the negative RF-bias during the pulsed direct current (DC) reactive magnetron sputtering process [16], modification of magnetic field in sputter apparatus [17], growing the films on the appropriate substrates [18, 19] and choosing proper seed layer [20]. Despite tremendous engineering efforts have been invested, the abnormal grains are still a major challenge for the growth of high quality piezoelectric $Sc_xAl_{1-x}N$ films.

These abnormal grains have been studied and confirmed as misoriented grains with the polar axis (*c*-axis) departing from the normal direction to the substrate surface [21–23], which is intuitively believed to reduce the material's piezoelectric response [24, 25]. Moreover, in mass production, the non-uniform distribution of the abnormal grains will lead to wafer level yield loss. Nevertheless, to date, there is still no systematic study about how the abnormal grains influence the performance of $Sc_xAl_{1-x}N$-based BAW resonators and filters quantitatively. The lack of the evaluation makes it difficult to predict the device performance and wafer-level uniformity based on the observed abnormal grain morphology, and also difficult to assess the wafer quality in terms of the abnormal grains.

In this work, for the first time, we systematically study the impact of the abnormal grains on the performance of the BAW devices by finite element modeling (FEM). Furthermore, the modeling results are compared with the measurements of devices on an 8 inch wafer, taking $Sc_{0.15}Al_{0.85}N$ BAW resonators and filters working at around 2.6 GHz as test vehicles. The density, dimension, and crystal orientation of the abnormal grains are correlated with the resonant frequency (f_s and f_p), k^2_{eff} and the quality factor of the resonator, as well as the bandwidth and insertion loss of the filter. This work provides a methodology to evaluate the impact of abnormal grains on the performance and yield of $Sc_{0.15}Al_{0.85}N$-based acoustic resonators and filters production. In addition, the simulation results can provide a guidance for the film optimization direction, but specific process approaches to suppress the abnormal grains are not discussed in this work.

2. Modeling of abnormal grains and discussion

2.1. Characterization of the abnormal grains

Before modeling, the morphology of the abnormal grains is appropriately described. ScAl alloy target with 15 at.% Sc is used to deposit the 1 μm thick $Sc_{0.15}Al_{0.85}N$ film via pulsed DC reactive magnetron sputtering on a sputtered 200 nm thick molybdenum (Mo) layer as the substrate. The locations of the abnormal grains on the 1 μm-thick $Sc_{0.15}Al_{0.85}N$ film are first identified on the image of the film surface captured by the defect review scanning electron microscopy. Then, the selected abnormal grain is cut by focused ion beam milling, before the cross-section of the abnormal grain is captured using transmission electron microscopy (TEM).

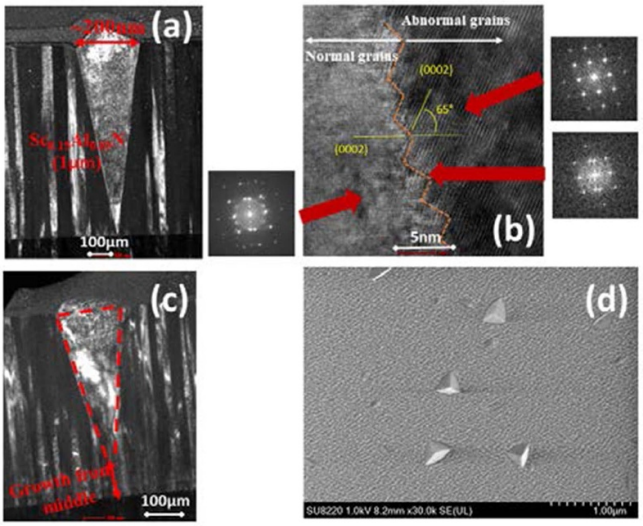

Figure 1. (a) Dark-field transmission electron microscopy (TEM) image of a typical cone-shape abnormal grain grown in the $Sc_{0.15}Al_{0.85}N$ film; (b) interface between normal and abnormal grains and the corresponding fast-Fourier-transformation (FFT) patterns; (c) dark-field TEM image of the abnormal grain which grows from middle of the film, about 10 nm departing from the bottom molybdenum (Mo) layer; (d) top view of the high magnification scanning electron microscopy (SEM) image of the film with abnormal grains. The cone-shape grains are clearly identified on the SEM photo.

The dark-field TEM image of a typical abnormal grain in the 1 μm thick $Sc_{0.15}Al_{0.85}N$ film is shown in figure 1(a). While the major proportions of the $Sc_{0.15}Al_{0.85}N$ film is columnar textured along the thickness direction, the abnormal grains can be identified as cone-shape crystallite grains, which nucleate near the bottom interface of the $Sc_{0.15}Al_{0.85}N$ layer, then grow through the entire film thickness with gradually enlarged size. The lateral size of the cone-shape grain on the top surface of the film is around 200 nm, while the height protruding from the film surface is around 50 nm. The grain boundary is further characterized and the high resolution TEM photo of the interface between the normal film and the abnormal grain is shown in figure 1(b), with the boundary highlighted with orange dash. By comparing the fast Fourier transform patterns of the regions on both sides of the boundary, it is indicated that both the normal film and the abnormal grain are of the Wurtzite structure. While the growth orientation of the normal grains is the [0002] orientation normal to the film surface, the [0002] orientation of the abnormal grains is found to be around 65° tilted from the normal direction to the film surface. It should be noted that the [0002] direction is the polar *c*-axis of the $Sc_xAl_{1-x}N$, along which the material has the strongest piezoelectric response. In some cases, the abnormal grains do not nucleate exactly from the bottom of the film, as shown in figure 1(c). The abnormal grain in this TEM photo starts growing at around 100 nm

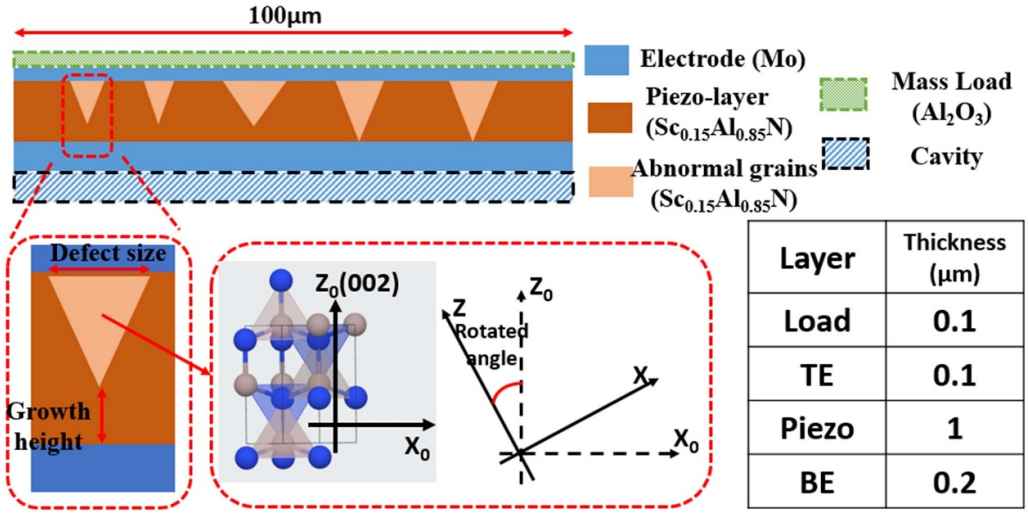

Layer	Thickness (μm)
Load	0.1
TE	0.1
Piezo	1
BE	0.2

Figure 2. Schematic of the device model for simulation. The stack configuration is shown in the parameter table. The abnormal grains are modeled as grains with tilted *c*-axis, which is the polar axis (002).

distance from bottom interface of the film. High magnification scanning electron microscopy (SEM) is utilized to observe the film surface, as shown in figure 1(d). The distribution of the abnormal grains is quite random within a typical resonator area (100 μm × 100 μm), and the dimension of the abnormal grains ranges from 0.1 μm to 0.4 μm.

2.2. Simulation setup

Considering the computational efficiency, two-dimensional FEM is utilized to simulate the performance of the $Sc_{0.15}Al_{0.85}N$-based film bulk acoustic resonator (FBAR) devices with abnormal grains. The film stack of the FBAR in this work is illustrated in figure 2. $Sc_{0.15}Al_{0.85}N$ piezoelectric film with 1 μm thick is sandwiched between a 0.1 μm and a 0.2 μm thick molybdenum (Mo) layer as the top electrode (TE) and the bottom electrode (BE), respectively. In some cases, an Al_2O_3 layer with 0.1 μm thickness is loaded above the top electrode to tune the resonant frequency of the FBAR for constructing the filters. The lateral size of the device is 100 μm.

Based on the micro observed morphology in figure 1, the abnormal grains are modeled as triangular $Sc_{0.15}Al_{0.85}N$ grains with tilted polar *c*-axis, as shown in figure 2. The polar axis of the normal grains is set along the *z*-axis in the model, and the abnormal grains are achieved by the rotation of the material around the out-of-plane *y*-axis, as shown in figure 2. The variable parameters of the abnormal grains considered in this work include the total count of the abnormal grains in the device, the size of the abnormal grains viewed from the top interface of the $Sc_{0.15}Al_{0.85}N$ layer, the distance between the bottom point of the cone-shape grains and the bottom film surface (referred as growth height) and the tilted angle of the *c*-axis of the abnormal grains. All the abnormal grains are randomly distributed over the entire device.

Frequency domain analysis was performed and the frequency responses of the impedance were plotted to evaluate the performance of the resonators. In the frequency spectrum, the minimum impedance is defined as the resonant impedance (R_s), and the corresponding frequency is defined as the resonant frequency (f_s); the maximum impedance is defined as the anti-resonant impedance (R_p) and the corresponding frequency is defined as the anti-resonant frequency (f_p). The effective coupling coefficient (k^2_{eff}) of the resonators is calculated by the formula below [26]:

$$k^2_{\text{eff}} = \frac{\pi}{2}\frac{f_s}{f_p}\cot\left(\frac{\pi}{2}\cdot\frac{f_s}{f_p}\right). \quad (1)$$

An ideal resonator has R_s of 0 Ω and R_p approaching infinity and the quality factor of the resonator is estimated by the R_p/R_s [27] in this work. To evaluate the change induced by the abnormal grains, relative R_s and relative R_p defined as the ratio of impedances of the resonator with abnormal grains to those of a defect-free resonator (referred to the resonator without any abnormal grains) are calculated in this work.

2.3. Results and discussion

The simulated impedance plots of the resonators with defect-free film and whole film tilted by 1 rad (about 57°) are shown in figure 3. Since the tilted polar axis departs from the applied electric field, k^2_{eff} is drastically reduced compared to the defect-free non-tilted film. Figures 4–7 show the simulated impedance plots and the calculated k^2_{eff}, relative R_s and relative R_p of the resonators versus respective parameters of the abnormal grains. The baseline of the controlled variables is setup as below: the count of the abnormal grains in the device is set to 40; the tilted angle of the *c*-axis is set to 1 rad (about 57°); the lateral size of the abnormal grain on the top surface is set to 0.3 μm; and the growth height of the abnormal grains is set to 0 μm. Figure 4 shows the simulation results of the impact of the abnormal grain count. With increasing count, more and more spurious modes appear around the f_s, accompanied with increasing R_s. That results in about 2% drop of the k^2_{eff} and

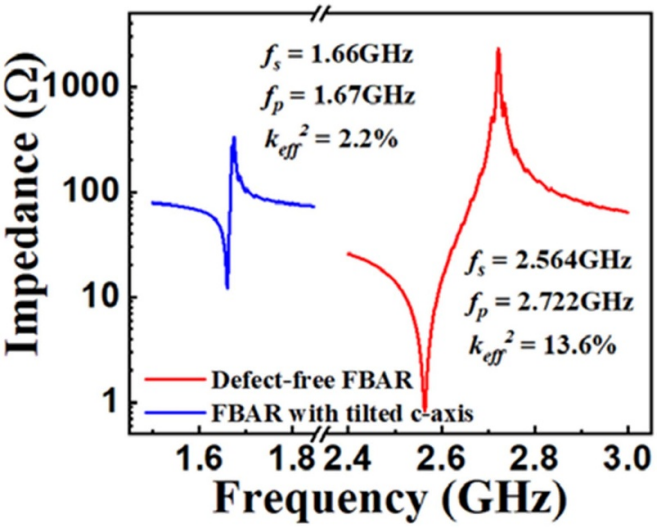

Figure 3. Simulation results of the BAW resonator with defect-free $Sc_{0.15}Al_{0.85}N$ film (red), and BAW resonator with the whole piezoelectric $Sc_{0.15}Al_{0.85}N$ film tilted (blue).

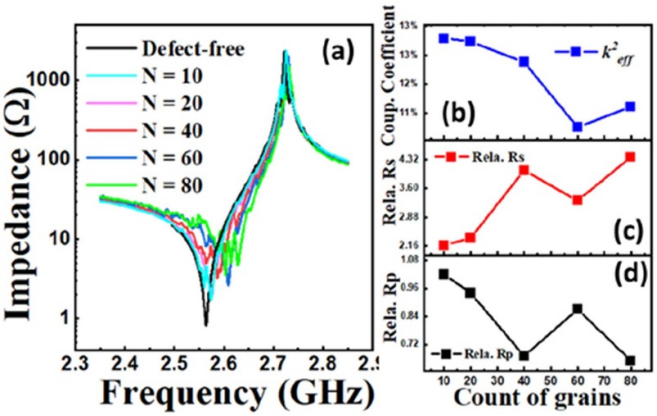

Figure 4. Simulation results of impact of abnormal grain count in the BAW resonator. The size of the abnormal grain is 0.3 μm, the tilted angle is 1 rad and the growth height is 0 μm. (a) Impedance-frequency curves; (b) k^2_{eff}; (c) relative R_{s}; (d) relative R_{p}.

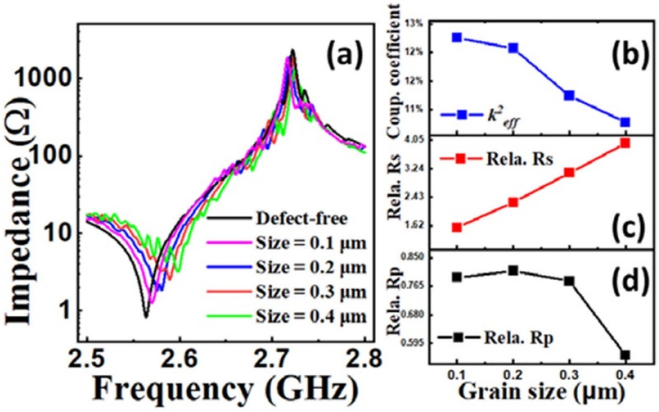

Figure 5. Simulation results of the impact of the abnormal grain size. The count of the abnormal grain is 40, the tilted angle is 1 rad and the growth height is 0. (a) Impedance-frequency curves; (b) coupling coefficient; (c) relative R_s; (d) relative R_p.

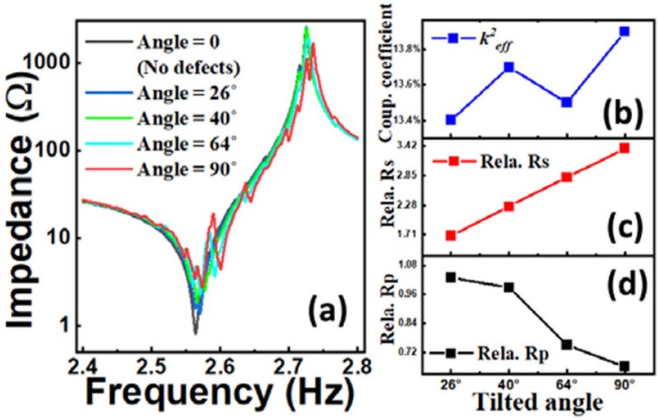

Figure 6. Simulation results of impact of tilted angle of the abnormal grains. The count of the abnormal grain is 40, the size of the abnormal grain is 0.3 μm, and the growth height is 0 μm. (a) Impedance-frequency curves; (b) k^2_{eff}; (c) relative R_{s}; (d) relative R_{p}.

the rising R_p/R_s. Figure 5 shows the impact of the size of the abnormal grains. The trend of the spurious modes, the relative R_s and the relative R_p is similar to the abnormal grain count. Figure 6 shows the impact of the tilted angle of c-axis. With the increasing tilted angle, though the ripples start to appear as expected, the k^2_{eff} does not suffer an obvious drop but fluctuates around 13.6%. The R_p/R_s has a clear decreasing trend with the increasing tilted angle. Figure 7 shows the simulated performance evolution of the resonator with varying growth height of the abnormal grains. With the increase of the growth height, the volume of each abnormal grain shrinks, resulting in the increase of the k^2_{eff}, the decrease of the relative R_s and the increase of the relative R_p.

The simulation results in figures 4–7 can be summarized that compared with the tilted angle of c-axis, the total volume of all the abnormal grains is more critical for the k^2_{eff}, R_s and R_p. The k^2_{eff} drops with the increase of the total volume of the abnormal grains, attributed to the count of the abnormal grains, the size of each grain or the growth height of each grain. The increased volume and tilted angle also induce spurious modes, which will impact the filter in-band loss and ripple. The increase of the relative R_{s} along with the decrease of relative R_{p} indicate the degradation of the quality factor with the increase of the total defective volume.

To investigate the impact of the morphology of the abnormal grains, we compare the abnormal grains with different combination of count and size, count and growth-height or abnormal grains growth in different layers, but with the same total volume in all scenarios. Figure 8 shows the comparison among different combinations of abnormal grain count and grain size while keeping the total volume in a single device as a constant. Figure 9 shows the comparison among different combinations of abnormal grain count and the growth point. Figure 10(a) shows the schematic of the abnormal grains growth in single and in two layers. Figure 10(b)

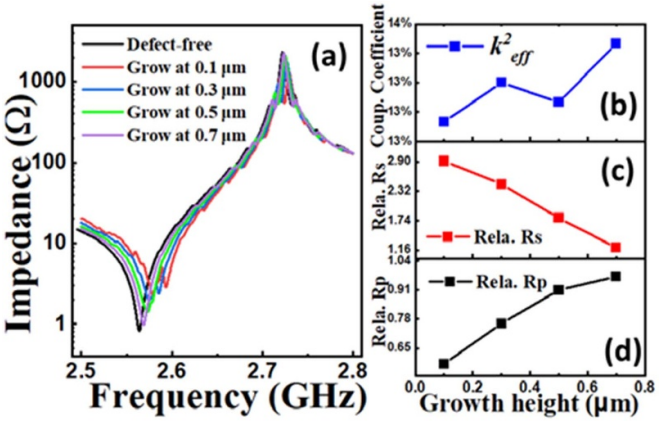

Figure 7. Simulation results of impact of the growth height of the abnormal grains. The count of the abnormal grain is 40, the size of the abnormal grain is 0.3 μm, and the tilted angle is 1 rad. (a) Impedance-frequency curves; (b) k^2_{eff}; (c) relative R_{s}; (d) relative R_{p}.

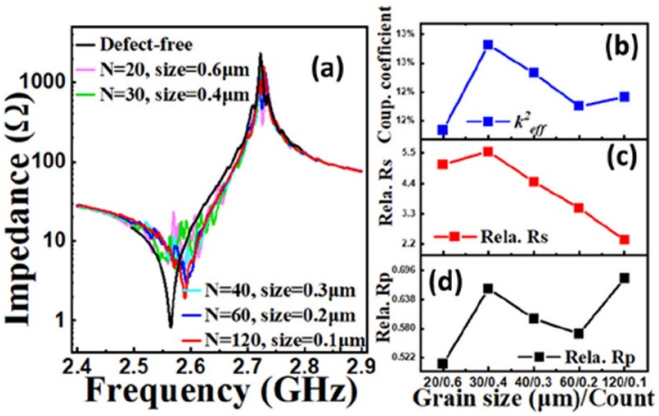

Figure 8. Simulation results of different abnormal grains morphology. The abnormal grains are with different combination of count and size but same total volume in a single device. (a) Impedance-frequency curves; (b) k^2_{eff}; (c) relative R_{s}; (d) relative R_{p}.

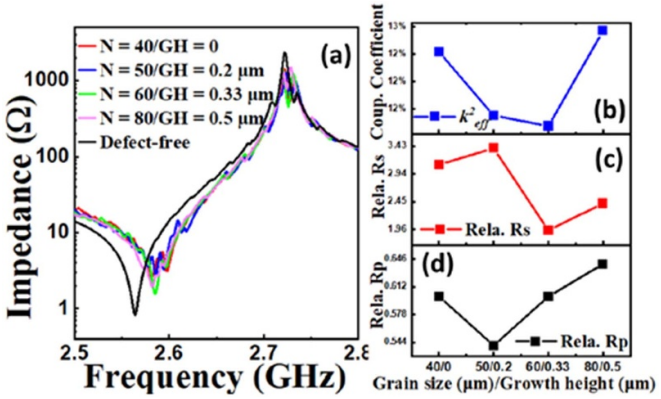

Figure 9. Simulation results of different abnormal grains morphology. The abnormal grains are with different combination of count and growth-height but same total volume in one device. (a) Impedance-frequency curves; (b) k^2_{eff}; (c) relative R_{s}; (d) relative R_{p}.

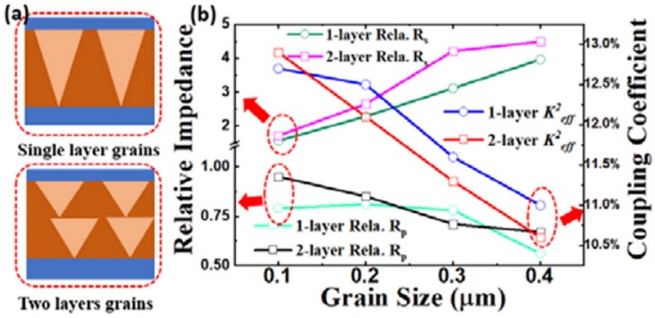

Figure 10. (a) Schematic of the abnormal grains growth in single and two layers; (b) simulated performance comparison of abnormal grains in single and two layers, including the k^2_{eff}, the relative R_{s} and relative R_{p}.

shows the comparisons of the k^2_{eff}, relative R_s and relative R_p between these two growth manners. In figures 8–10, the actual comparison is between the case with larger but less grains and the case with smaller but more grains, while keeping the total volume constant. Since no obvious trend can be concluded in the comparisons, the results in figures 8–10 indicate that in contrast of heavy dependence of the resonator performance on the total volume of the abnormal grains, the morphology change only brings subtle fluctuations to the resonator performance.

The abnormal grains in the aforementioned simulations are all constructed identically in each device to investigate the impact of each variable parameter. However, in the realistic resonator devices, the abnormal grains diverse from one another. Therefore, a statistic study needs to be conducted to predict the performance of the realistic resonators with abnormal grains. To obtain the statistic impact of the abnormal grains, 120 resonators with random count and individually randomly featured (size, tilted angle and growth height) abnormal grains were simulated. The abnormal grain count and the growth height are uniformly distributed from 20 to 80 and from 0 to 0.4 μm, respectively; the tilted angle and grain size follow the Gaussian distribution with mean tilted angle $\mu_{\text{angle}} = 2/3\pi$, standard derivation $\sigma_{\text{angle}} = \pi/6$ and mean grain size $\mu_{\text{size}} = 0.25$ μm, standard derivation $\sigma_{\text{size}} = 0.15$ μm, respectively. Simulated distribution of BAW resonator performance with random abnormal grain configuration is shown in figure 11. Figure 11(a) shows the distribution of the resonant and anti-resonant frequency, with the f_s and f_p of the FBAR marked as reference. The impact of the abnormal grains on f_s is obviously larger than that on f_p; and with the randomly featured abnormal grains, f_s and f_p almost evenly distribute on both sides of the reference. Figure 11(b) shows the statistic results of the k^2_{eff}. Over 90% of the devices with abnormal grains suffer a degradation of the k^2_{eff} with an average k^2_{eff} of 12.4%. Figure 11(c) shows the distribution of the relative R_s and R_p. An average of 3-time raising of the R_s is observed and the average relative R_p is around 0.9. As a conclusion, with the average total volume of the abnormal grains being calculated to be about 6% of the volume of the entire piezoelectric layer,

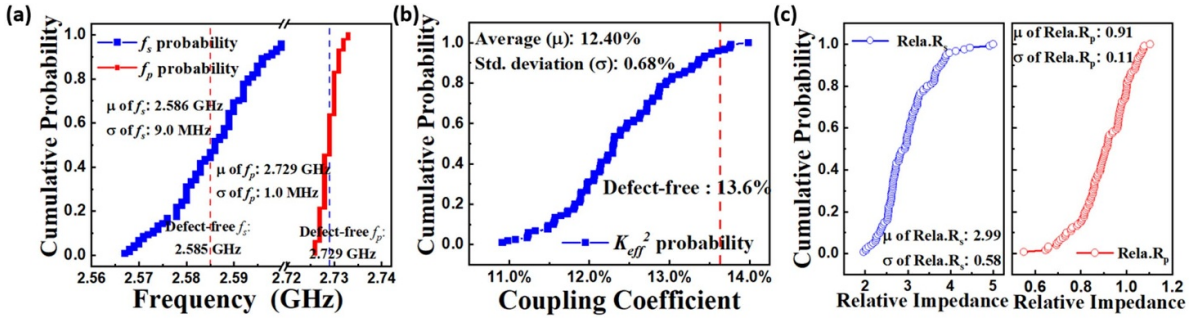

Figure 11. Simulated distribution of BAW resonator performance with random abnormal grain configuration (count, angle, size and growth height). (a) f_s and f_p; (b) k^2_{eff}; (c) relative R_s and relative R_p. The abnormal grain count is uniformly distributed from 20 to 80, the growth height is uniformly distributed from 0 to 0.4 μm; the tilted angle and grain size follow the Gaussian distribution with $\mu = 2/3\pi$, $\sigma = \pi/6$ and $\mu = 0.25$ μm, $\sigma = 0.15$ μm, respectively. The average volume of the abnormal grains about 6% of the total piezoelectric layer.

the simulation results indicate that the variation of f_s and R_s induced by the random abnormal grains is larger than that of f_p and R_p, and the k^2_{eff} could degrade from 13.6% to an average value of 12.4% and as low as 11% in some cases.

3. Measurements on 8 inch wafer

3.1. Process and experiments

To validate the simulation results, $Sc_{0.15}Al_{0.85}N$-based BAW resonators and filters are designed and fabricated on an 8-inch wafer [28], with the stack thickness configuration same as the simulation setup in figure 2. Tetraethyl orthosilicate (TEOS) SiO_2 is first prepared on the high resistivity Si substrate as the isolation layer, followed by photolithography to define the release barrier with a trench surrounding the resonator area. The trench is then etched and subsequently filled by Low pressure chemical vapor deposition (LPCVD) Si, followed by chemical mechanical polishing to expose the SiO_2. Then bottom Mo layer, $Sc_{0.15}Al_{0.85}N$ layer and the top Mo layer are deposited using DC magnetron sputtering in sequence. In some resonators, an additional Al_2O_3 layer is then deposited by atomic layer deposition as the mass loading layer. Next, an Aluminum layer is deposited and patterned on the probing pads of each resonator and filter for better electrical contact. Finally, the release holes for vapor Hydrogen fluoride (VHF) flow are etched and the cavity defined by the trench is released. The top-view photo and cross-section schematic of the fabricated resonator are shown in figure 12. Electrical testing of the fabricated resonators and filters are performed in a FormFactor CM300xi 300 mm semi-automated shielded probe system with a Keysight N5244B PNA-X Microwave Network Analyzer. Since the nucleation of the abnormal grains is related to the fluctuation of the local stress [14, 15], the density and morphology of abnormal grains in each resonator vary at different locations within the same wafer. Generally, the density mainly depends on the distance from the center of the wafer, larger density is obtained with resonator closer to the edge of the wafer. The SEM images of 10 μm × 10 μm area on the top plate of the resonators are captured to identify the abnormal grain density and morphology, as well as to represent the density of abnormal grains in the corresponding resonator.

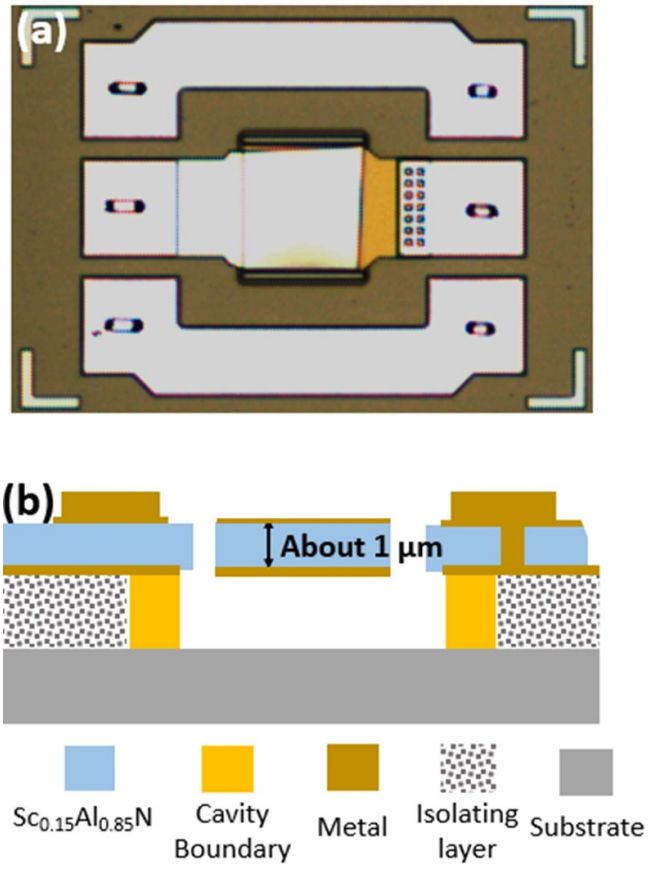

Figure 12. (a) Top-view photo and (b) cross-section schematic of the fabricated BAW resonator.

3.2. Results and discussions

The typical impedance plots of the resonators with different levels of abnormal grains density are shown in figure 13(a), while figures 13(b)–(d) are the corresponding SEM images of the morphology of the abnormal grains in the selected resonators in figure 13(a). With a low density of abnormal grains (<10 per 100 μm^2, as shown in figure 13(b)), the k^2_{eff} (13.4%) is quite consistent with the simulation result (13.6%) of the resonator without any abnormal grains, meaning that at

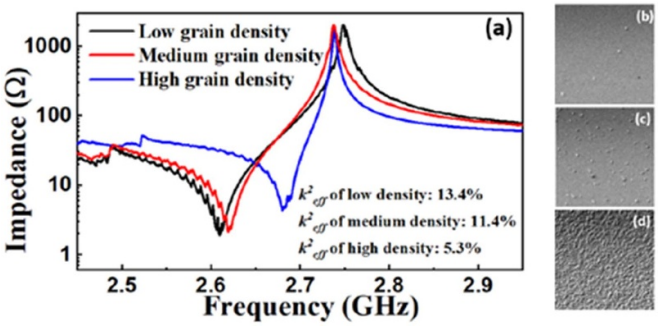

Figure 13. (a) Measured impedance plot of the BAW resonators with different abnormal grains density; (b)–(d) SEM photos of the top view of the BAW resonators with different abnormal grain density. (b) Low density; (c) medium density; (d) high density.

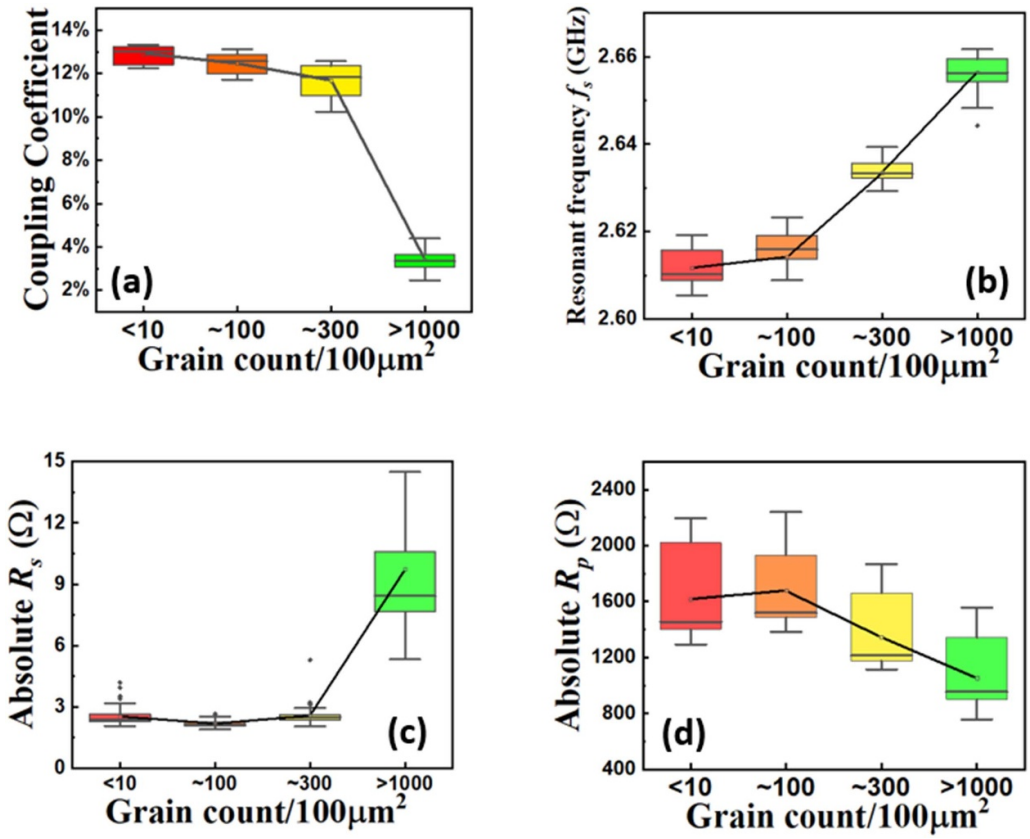

Figure 14. Measured distributions of the BAW resonators performances (k^2_{eff}; f_s, R_s, and R_p) on an 8 inch wafer. Devices are categorized by the abnormal grain density. (a) k^2_{eff}; (b) f_s; (c) R_s; (d) R_p.

this density level the abnormal grain has nearly no impact on the resonator performance. With a medium density of abnormal grains (∼100 per 100 μm^2, as shown in figure 13(c)), the k^2_{eff} slightly reduces to 11.4%. While in the high-density case shown in figure 13(d), the k^2_{eff} is dramatically reduced to less than 6%, accompanied with an obvious increase of the R_s.

To experimentally obtain the general evaluation of the abnormal grains on the fabricated resonators, the resonators should be appropriately categorized based on the abnormal grain status and statistically analyzed. 69 resonators evenly distributed on the whole wafer are selected for the correlation between the abnormal grains and the electrical characteristics. Similar with figure 13, the resonators are categorized by the count of abnormal grains in the 100 μm^2 area captured by SEM. The box chart of the distribution of the k^2_{eff}, f_s, R_s and R_p of the selected resonators is shown in the figure 14. The statistic results show that with the abnormal grain density smaller than 100 per 100 μm^2, the reduction of the k^2_{eff} is less than 1% and the shift of f_s is less than 100 MHz. Obvious performance degradation, such as 1%–2% k^2_{eff} degradation, over 300 MHz f_s shift, and 25% R_p/R_s degradation, is observed in the resonators with around 300 abnormal grains per 100 μm^2. With abnormal grain density over 1000 per 100 μm^2, the average k^2_{eff} of the resonators dramatically drop to less than 5%, along with R_p/R_s reduced to ∼20%.

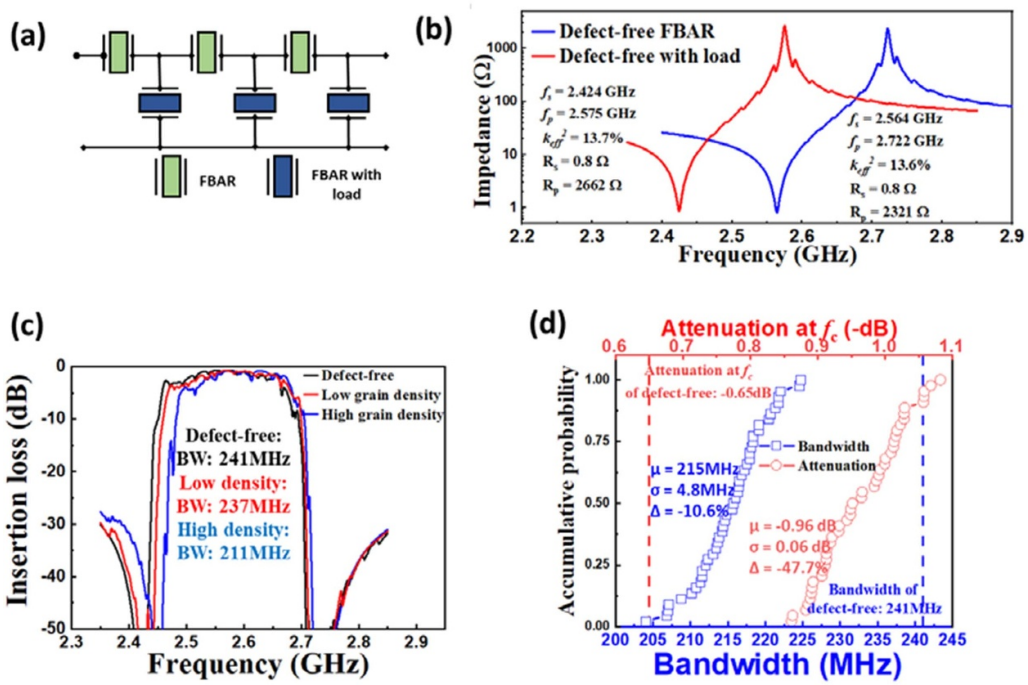

Figure 15. (a) The ladder filter structure; (b) BAW resonators with and without mass load layer; (c) simulated insertion loss of the filter composed of resonators with abnormal grains; (d) distribution of the bandwidth and insertion loss at center frequency.

It should be noted that although the analysis in this section is based on the density of the abnormal grains, an implicit assumption made from the SEM and TEM images is that the size and the growth height of the abnormal grains are normally distributed, and the average values are close in different areas of the wafer. Thus, the total volume of the abnormal grains can be represented by the count density. Based on the SEM observation, with the average dimension of 0.25 μm on the top surface, the average volume of a single cone-shape abnormal grain is estimated to be 0.018 μm^3. The volume of 300 abnormal grains is then 5.34 μm^3, corresponding to 5.3% of the total volume of the film with 100 μm^2 area and 1 μm thickness. The ratio is close to the simulation setup in figure 11, and for the 300 count/100 μm^2 group in figure 14, the degradation of k^2_{eff} is around 2%, which is quite consistent with the simulation results. Generally speaking, the statistic measurement results show the decrease of the k^2_{eff} and R_p/R_s with the increase total volume of the abnormal grains, demonstrating good agreement with the trends summarized in the simulations.

4. Ladder filters with abnormal grains

Since RF resonators are the basic components of RF filters, it is important to investigate the impact of the abnormal grains on the $Sc_{0.15}Al_{0.85}N$-based filters. Figure 15(a) shows the topology of the ladder filters deployed in this work, consisting of three series resonators and three shunt resonators. Mass loading layer is added on the shunt resonators to tune the anti-resonant frequency to be slightly higher than the f_s of the series resonator. Figure 15(b) shows the impedance plots of the series and shunt resonators without any abnormal grains. The simulated insertion loss variation of the ladder filters composed of resonators without and with different abnormal grain densities are shown in figure 15(c). The derived bandwidth of the corresponding filters is also labeled in the figure. The results show that with the increase of the abnormal grain density, the center frequency shifts upwards while the bandwidth of the filter shrinks. Since the bandwidth of the filters mainly depends on the k^2_{eff} of the composing resonators, this trend can be intuitively inferred from the reduction of the k^2_{eff} induced by the abnormal grains.

Fifty ladder filters with randomly distributed abnormal grains added into both series and parallel resonators are simulated to obtain a statistical impact of the abnormal grains on the filter performance. In this simulation, the setup of the abnormal grains in all resonators is the same with the random configuration in section 2. The performance distributions of the filters illustrated in figure 15(d) indicates an average 10.6% decrease of bandwidth, compared to the filters composed of abnormal-grain-free resonators. Also, because of the reduction of R_p/R_s, which can represent the quality factor, the insertion loss at the center frequency of the pass band is averagely degraded by 47.7% with the existence of the abnormal grains. The reduction of both bandwidth and insertion loss, as well as the nonuniformity induced by the abnormal grains, put forward higher requirements for the system design of the modules.

5. Conclusion

In this work, the impact of the abnormal grains in the $Sc_{0.15}Al_{0.85}N$ film on the performance of BAW resonators and filters have been systematically evaluated and verified by the measurements on an 8 inch wafer. Results show that the k^2_{eff}

of the resonators and the bandwidth of the filters will decrease with the increase of the total volume of the abnormal grains. 120 resonators with an average of 6% volume of the film occupied by abnormal grains are simulated and the results show that resonators' k^2_{eff} suffers over 2% degradation and thus 10.6% decrease for the bandwidth of the filters. This work provides a numerical estimation of the performance degradation induced by the abnormal grains and a practical guideline for the $Sc_xAl_{1-x}N$ film optimization: minimizing the total volume of the abnormal grains should be the goal for process development.

Data availability statement

All data that support the findings of this study are included within the article (and any supplementary files).

Acknowledgments

This work was supported by the Science and Engineering Research Council of A*STAR (Agency for Science, Technology and Research), Singapore, under Grant No. (A20G9b0135).

References

[1] Aigner R, Fattinger G, Schaefer M, Karnati K, Rothemund R and Dumont F 2019 BAW filters for 5G bands *Tech. Dig.—Int. Electron Devices Meeting (IEDM)* (*December 2018*) pp 14.5.1–4

[2] Hagelauer A, Fattinger G, Ruppel C C W, Ueda M, Hashimoto K Y and Tag A 2018 Microwave acoustic wave devices: recent advances on architectures, modeling, materials, and packaging *IEEE Trans. Microwave Theory Tech.* **66** 4548–62

[3] Ruppel C C W 2017 Acoustic wave filter technology-a review *IEEE Trans. Ultrason. Ferroelectr. Freq. Control* **64** 1390–400

[4] Wang N, Zhu Y, Chen B and Zhang Y Over 12% of coupling coefficient demonstrated by 3GHz $Sc_{0.12}Al_{0.88}N$ based laterally coupled alternating thickness (LCAT) mode resonators *IEEE Int. Ultrason. Symp. IUS* (*October 2019*) pp 1971–3

[5] Wang N *et al* 2019 Over 10% of k^2_{eff} demonstrated by 2-GHz spurious mode-free $Sc_{0.12}Al_{0.88}N$ laterally coupled alternating thickness mode resonators *IEEE Electron Device Lett.* **40** 957–60

[6] Zhu Y, Wang N, Chua G, Sun C, Singh N and Gu Y 2017 ScAlN-based LCAT mode resonators above 2 GHz with high FOM and reduced fabrication complexity *IEEE Electron Device Lett.* **38** 1481–4

[7] Liu C, Zhu Y, Wang N and Chen B 2021 Single-chip dual-band filters based on spurious-free dual-resonance $Sc_{0.15}Al_{0.85}N$ laterally coupled alternating thickness (LCAT) mode resonators *2021 21st Int. Conf. Solid-State Sensors, Actuators and Microsystems (Transducers)* pp 309–12

[8] Kurz N, Ding A, Urban D F, Lu Y, Žukauskaitė A and Ambacher O 2019 Experimental determination of the electro-acoustic properties of thin film AlScN using surface acoustic wave resonators *J. Appl. Phys.* **126** 075106

[9] Akiyama M, Umeda K, Honda A and Nagase T 2013 Influence of scandium concentration on power generation figure of merit of scandium aluminum nitride thin films *Appl. Phys. Lett.* **102** 021915

[10] Akiyama M, Kamohara T, Kano K, Teshigahara A, Takeuchi Y and Kawahara N 2009 Enhancement of piezoelectric response in scandium aluminum nitride alloy thin films prepared by dual reactive cosputtering *Adv. Mater.* **21** 593–6

[11] Fichtner S, Wolff N, Krishnamurthy G, Petraru A, Bohse S, Lohfink F, Chemnitz S, Kohlstedt H, Kienle L and Wagner B 2017 Identifying and overcoming the interface originating *c*-axis instability in highly Sc enhanced AlN for piezoelectric micro-electromechanical systems *J. Appl. Phys.* **122** 035301

[12] Sandu C S, Parsapour F, Mertin S, Pashchenko V, Matloub R, LaGrange T, Heinz B and Muralt P 2019 Abnormal grain growth in AlScN thin film induced by complexion formation at crystallite interfaces *Phys. Status Solidi* a **216** 1800569

[13] Bogner A, Timme H, Bauder R, Mutzbauer A, Pichler D, Krenzer M, Reccius C, Weigel R and Hagelauer A 2019 Impact of high sc content on crystal morphology and RF performance of sputtered $Al_{1-x}Sc_xN$ SMR BAW *IEEE Int. Ultrasonics Symp. IUS (IUS)* (*October 2019*) pp 706–9

[14] Henry M D, Young T R, Douglas E A and Griffin B A 2018 Reactive sputter deposition of piezoelectric $Sc_{0.12}Al_{0.88}N$ for contour mode resonators *J. Vac. Sci. Technol.* B **36** 03E104

[15] Fichtner S, Reimer T, Chemnitz S, Lofink F and Wagner B 2015 Stress controlled pulsed direct current co-sputtered $Al_{1-x}Sc_xN$ as piezoelectric phase for micromechanical sensor applications *APL Mater.* **3** 116102

[16] Sandu C S, Parsapoura F, Xiaoa D, Nigona R, Riemerd L M, LaGrangec T and Muralta P 2020 Impact of negative bias on the piezoelectric properties through the incidence of abnormal oriented grains in $Al_{0.62}Sc_{0.38}N$ thin films *Thin Solid Films* **697** 137819

[17] Yeh T, Nikkel P, Grannen K J, Feng C and Choy J 2015 Fabricating low- defect rare-earth doped piezoelectric layer *US Patent 2015/0311046 A1* October

[18] Esteves G, Berg M, Wrasman K D, David Henry M, Griffin B A and Douglas E A 2019 CMOS compatible metal stacks for suppression of secondary grains in $Sc_{0.125}Al_{0.875}N$ *J. Vac. Sci. Technol.* A **37** 021511

[19] Mertin S, Heinz B, Rattunde O, Christmann G, Dubios M, Nicolay S and Muralt P 2018 Piezoelectric and structural properties of *c*-axis textured aluminium scandium nitride thin films up to high scandium content *Surf. Coat. Technol.* **343** 2–6

[20] Felmetsger V, Mikhov M, Ramezani M and Tabrizian R 2019 Sputter process optimization for $Al_{0.7}Sc_{0.3}N$ piezoelectric films *IEEE Int. Ultrasonics Symp., IUS* (*October*) pp 2600–3

[21] Li M, Xie J, Chen B, Wang N and Zhu Y 2019 Microstructural evolution of the abnormal crystallite grains in sputtered ScAlN film for piezo-MEMS applications *IEEE Int. Ultrasonics Symp., IUS* (*October*) pp 1124–6

[22] Li M, Hu K, Lin H and Zhu Y 2021 Structural characterization of the abnormal grains evolution in sputtered ScAlN films *2021 IEEE Int. Ultrasonics Symp. (IUS)* pp 16–18

[23] Muralt P, Pashchenko V, Parsapour F, Mertin S, Heinz B and Nicolay P 2019 Growth, properties, and applications of $Al_{1-x}Sc_xN$ thin films *IEEE Int. Ultrasonics Symp., IUS* (*October*) pp 255–7

[24] Parsapour F, Pashchenko V, Kurz N, Sandu C S, LaGrange T, Yamashita K, Lebedev V and Muralt P 2019 Material parameter extraction for complex AlScN thin film using dual mode resonators in combination with advanced

microstructural analysis and finite element modeling *Adv. Electron. Mater.* **5** 1800776
[25] Lu Y, Reusch M, Kurz N, Ding A, Christoph T, Kirste L, Lebedev V and Zukauskaite A 2018 Surface morphology and microstructure of pulsed DC magnetron sputtered piezoelectric AlN and AlScN thin films *Phys. Status Solidi* **215** 1700559
[26] Aigner R 2007 Bringing BAW technology into volume production: the ten commandments and the seven deadly sins *Proc. 3rd Int. Symp. Acoustic Wave Devices for Future Mobile Communication Systems* (*Chiba, Japan*, *March*)
[27] Bi F Z and Barber B P 2008 Bulk acoustic wave RF technology *IEEE Microwave Mag.* **9** 65–80
[28] Wang N, Zhu Y, Chua G L, Chen B, Srinivas M, Singh N and Gu Y 2018 Spurious mode free 3.5GHz AlN plate mode resonator with high FOM *2018 IEEE Int. Ultrasonics Symp. (IUS)* pp 1–4